The current issue and full text archive of this journal is available at
www.emeraldinsight.com/0961-5539.htm

The computation of flow and heat transfer through an orthogonally rotating square-ended U-bend, using low-Reynolds-number models

Konstantinos-Stephen P. Nikas
Laboratory of Aerodynamics, Department of Mechanical Engineering, National Technical University of Athens, Athens, Greece, and
Hector Iacovides
School of Mechanical, Aerospace and Civil Engineering, The University of Manchester, Manchester, UK

Abstract

Purpose – To assess how effectively two-layer and low-Reynolds-number models of turbulence, at effective viscosity and second-moment closure level, can predict the flow and thermal development through orthogonally rotating U-bends.

Design/methodology/approach – Heat and fluid flow computations through a square-ended U-bend that rotates about an axis normal to both the main flow direction and also the axis of curvature have been carried out. Two-layer and low-Reynolds-number mathematical models of turbulence are used at effective viscosity (EVM) level and also at second-moment-closure (DSM) level. In the two-layer models the dissipation rate of turbulence in the new-wall regions is obtained from the wall distance, while in the low-*Re* models the transport equation for the dissipation rate is extended right up to the walls. Moreover, two length-scale correction terms to the dissipation rate of turbulence are used with the low-*Re* models, and original Yap term and a differential form that does not require the wall distance (NYap). The resulting predictions are compared with available flow measurements at a Reynolds number of 100,000 and a rotation number ($\Omega D/U_b$) of 0.2 and also with heat transfer measurements at a Reynolds number of 36,000, rotation number of 0.2 and Prandtl number of 5.9 (water).

Findings – While the main flow features are well reproduced by all models, the development of the mean flow within the just after the bend in better reproduced by the low-*Re* models. Turbulence levels within the rotation U-bend are under-predicted, but DSM models produce a more realistic distribution. Along the leading side all models over-predict heat transfer levels just after the bend. Along the trailing side, the heat transfer predictions of the fully low-*Re* DSM with the differential length-scale correction term NYap are close to the measurements, with an average error of around 10 per cent, though at the bend exit it rises to 25 per cent. The introduction of a differential form of the length-scale correction term to improve the heat transfer predictions of both low-*Re* models.

Research/limitations/implications – The numerical models assumed that the flow remains steady and is not affected by large-scale, low frequency fluctuations. Unsteady RANS computations or LES must also be tested in the future.

Originality/value – This work has expanded the range of complex turbulent flow over which the effectiveness of RANS models has been tested, to internal cooling flows simultaneously affected by orthogonal rotation and strong curvature.

Keywords Heat transfer, Rotational motion, Flow, Turbulent flow

Paper type Research paper

International Journal of Numerical Methods for Heat & Fluid Flow
Vol. 16 No. 7, 2006
pp. 827-844

0961-5539
DOI 10.1108/09615530610683539

Introduction

Tight square-ended U-bends, shown in Figure 1, can be considered as an idealised representation of the tight turns present in internal cooling passages of gas-turbine blades. The flow inside these cooling passages is complex and highly three-dimensional, influenced by the presence of the sharp U-bends, surface rib-roughness and also by the rotation of the blades. The axis of rotation is normal to the main flow direction, known as orthogonal rotation, and in relation to the U-bend its orientation tends to be closer to that shown in Figure 1(a) where it is normal to the axis of curvature. The optimisation of such passages could greatly benefit from the use of numerical flow solvers that can reliably simulate the flow and thermal development within them. The development of such solvers requires the use of mathematical models of turbulence that can reproduce the effects of strong curvature, rib roughness and rotation on the turbulence field. In this contribution we look at the numerical simulation of flows that contain two of the three main features present in blade cooling passages, namely strong curvature and orthogonal rotation.

Flow and heat transfer through tight U-bends, with and without rotation, have been the subject of a number of recent experimental and numerical investigations such as those of Ekkad and Han (1995) and Rigby *et al.* (1996). In the authors' group, previous numerical investigations and most earlier experimental studies focused on round-ended U-bends, shown in Figure 1(b), Bo *et al.* (1995) and Iacovides *et al.* (1995). These studies employed low-Reynolds-number models at both effective-viscosity and second-moment closure levels. They showed that all turbulence models used, predicted a later separation along the inner wall of the bend than what is indicated by the experimental data. The introduction of second-moment closures was shown to lead to considerable improvements in the prediction of flow separation. In the case of square-ended U-bend, in addition to the strong curvature, the presence of the sharp 90°-corners along the outer wall and the continuous change in cross-sectional area also influence the flow and thermal developments. The recent emergence of local flow and thermal data for square-ended U-bends from our group, Iacovides *et al.* (1999) and also from other groups, provided the validation data necessary to assess the effectiveness of turbulence models under these more complex conditions. As we have recently reported. Nikas and Iacovides (2004), in the prediction of flow and heat transfer in stationary square-ended U-bends, effective-viscosity and second-moment closures returned very similar flow predictions, both under-predicting the separation bubble at the bend exit. Some differences were

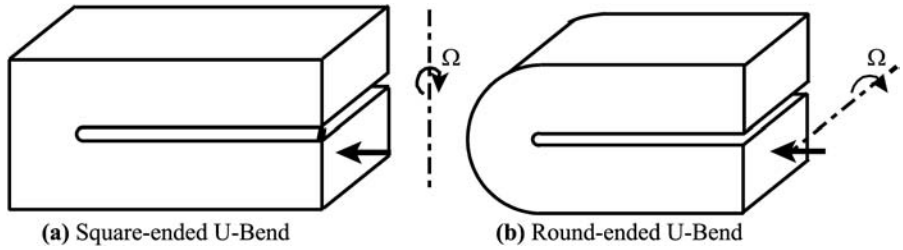

Figure 1.
Flow geometries and modes of rotation

observed in the predictions of wall heat transfer, with the low-*Re* second-moment closure producing the more reliable simulations.

Here, attention is focused on flow and heat transfer through square-ended U-bends that rotate orthogonally about an axis-normal to that of curvature, as shown in Figure 1(a). The objective is to use the same models of turbulence employed in our earlier studies of flows through round- and square-ended U-bends and also through ribbed passages, Iacovides and Raisee (1999), in order to assess their effectiveness in predicting the flow and thermal development in rotating square-ended U-bends. These models include two-layer and low-*Re* models at both effective-viscosity and second-moment closure level.

Theoretical model

The flow computations have been obtained through the solution of the Reynolds-averaged flow equations, presented here in Cartesian tensor notation, for a rotating frame of reference:

$$\text{Continuity}: \quad \frac{\partial}{\partial x_i}(\rho U_i) = 0 \tag{1}$$

$$\text{Momentum}: \quad \frac{\partial}{\partial x_j}(\rho U_j U_i) = -\frac{\partial P}{\partial x_i} + \frac{\partial}{\partial x_j}\left[\mu\left(\frac{\partial U_i}{\partial x_j} + \frac{\partial U_j}{\partial x_i}\right) - \rho\overline{u_j u_i}\right] - 2\rho\varepsilon_{ijp}\Omega_p U_j - \rho[\Omega_j X_j \Omega_i - \Omega_j X_i \Omega_j] \tag{2}$$

$$\text{Energy}: \quad \frac{\partial}{\partial x_j}(\rho T) = \frac{\partial}{\partial x_j}\left[\frac{\mu}{\text{Pr}}\frac{\partial T}{\partial x_j} - \rho\overline{u_i t}\right] \tag{3}$$

In equation (2) above, Ω_p denotes the rotation vector of the co-ordinate system and X_i the position vector relative to the axis of rotation. The first group of rotation terms in equation (2) represent the Coriolis forces and the second group the centrifugal forces. The flows computed here are water flows that are either isothermal or involve temperature differences small enough for the density to be practically constant. The centrifugal terms, therefore, do not influence the flow development.

Turbulence modelling

Effective viscosity models. Two EVM models have been used, a two-layer k-ε/one-equation model and a low-*Re* k-ε model. In both versions, the Reynolds stresses and the turbulent heat fluxes are obtained from the effective viscosity and effective diffusivity approximations, respectively. The effective viscosity approximation is used because of its numerical robustness, even though this simplicity is known to result in turbulence stress fields that are close to isotropic, especially when normal straining is weak and also stress fields insensitive to the effects of streamline curvature and rotation:

$$\rho\overline{u_j u_i} = \frac{2}{3}k\delta_{ij} - \mu_t\left(\frac{\partial U_i}{\partial x_j} + \frac{\partial U_j}{\partial x_i}\right) \tag{4}$$

$$\overline{u_i t} = -\frac{\mu_t}{\sigma_\text{T}}\frac{\partial T}{\partial x_i} \tag{5}$$

The two-layer EVM model consists of the standard high-*Re* version in the fully-turbulent region, matched to Wolfshtein's (1969) low-*Re* one-equation model of *k*-transport in the near-wall regions. This approach allows the resolution of the mean flow across the viscous wall sub-layer without the need to use an excessively fine near-wall grid. The equations involved are widely used and are thus not presented here due to space limitations.

The low-*Re* EVM model employed is Launder and Sharma's (1974) well known extension of the high-*Re* k-ε that can reproduce the wall damping of turbulence and hence can be used across the viscous sub-layer. Again the widely used equations involved are not included here for brevity.

The equations for the low-*Re* DSM model are:

$$\frac{\partial}{\partial x_k}(\rho U_k \overline{u_i u_j}) = \frac{\partial}{\partial x_k}\left[\left(\mu + \frac{\mu_t}{\sigma_k}\right)\frac{\partial \overline{u_i u_j}}{\partial x_k}\right] + P_{ij} - \rho\varepsilon_{ij} + \varphi_{ij} - \left[H_{ij} - \frac{1}{3}H_{kk}\delta_{ij}\right] + J_{ij} \quad (6)$$

$$P_{ij} = -\rho\left(\overline{u_i u_k}\frac{\partial U_j}{\partial x_k} + \overline{u_j u_k}\frac{\partial U_i}{\partial x_k}\right) - 2\rho\Omega_p(\varepsilon_{ipq}\overline{u_q u_j} + \varepsilon_{jpq}\overline{u_q u_i}) \quad (7)$$

$$\varepsilon_{ij} = \frac{2}{3}(1 - f_\varepsilon)\varepsilon\delta_{ij} + f_\varepsilon\frac{\overline{u_i u_j}}{k}\varepsilon \quad (8)$$

$$\varphi_{ij} = -c_1\frac{\varepsilon}{k}\left(\overline{u_i u_j} - \frac{2}{3}k\delta_{ij}\right) - c_2\left(P_{ij} - \frac{2}{3}P_k\delta_{ij}\right) + f_w\left(\varphi^w_{ij,1} + \varphi^w_{ij,2}\right) \quad (9)$$

$$\varphi^w_{ij,1} = -c^w_1\frac{\varepsilon}{k}\left(\overline{u_k u_m}n_k n_m\delta_{ij} - \frac{3}{2}\overline{u_k u_i}n_k n_j - \frac{3}{2}\overline{u_k u_j}n_n n_i\right)\left\{\frac{k^{1.5}}{\varepsilon c_l x_n}\right\} \quad (10)$$

$$\varphi^w_{ij,2} = c^w_2\frac{\varepsilon}{k}\left(\varphi_{km2}n_k n_m\delta_{ij} - \frac{3}{2}\varphi_{ik2}n_k n_j - \frac{3}{2}\varphi_{jk2}n_k n_i\right)\left\{\frac{k^{1.5}}{\varepsilon c_l x_n}\right\} \quad (11)$$

$$\text{where } \varphi_{ij2} = -c_2\left(p_{ij} - \frac{2}{3}P_k\delta_{ij}\right) \quad (12)$$

$$H_{ij} = f_H\frac{v}{k}\left(\overline{u_i u_l}\frac{\partial\sqrt{k}}{\partial x_l}\frac{\partial\sqrt{k}}{\partial x_j} + \overline{u_j u_l}\frac{\partial\sqrt{k}}{\partial x_l}\frac{\partial\sqrt{k}}{\partial x_i}\right) \quad (13)$$

$$J_{ij} = f_j k\left(\frac{\partial U_i}{\partial x_j} + \frac{\partial U_j}{\partial x_i}\right) \quad (14)$$

$$\overline{u_i t} = -\rho c_T\frac{k}{\varepsilon}\overline{u_i u_j}\frac{\partial T}{\partial x_j} \quad (15)$$

In the above equations, k, ε, l, n, J and T in σ_k, f_ε, c_l, x_n, f_J and $c_?$, are all subscripts and not tensorial indices.

Low-Re *DSM models*. The DSM closures employed here are rather simple and empirically derived extensions to the basic DSM model that relies on the linear redistribution terms and use the wall reflection terms. They have evolved from the low-*Re* ASM closures proposed by Iacovides and Launder (1992) and were initially applied to flow and heat transfer through U-bends of mild curvature. They were

subsequently extended by Iacovides and Toumpanakis (1993) to low-*Re* DSM closures and were first used for the computation of turbulent flows through rotating cavities (Iacovides *et al.* 1996), where they produced satisfactory predictions. Iacovides and Raisee (1999, 2001) have also applied these low-*Re* DSM closures more recently to the computation of flow and heat transfer through ribbed passages, where again their introduction improved the thermal predictions. More recently, we have also used these models in the computation of heat and fluid flow through stationary U-bends with encouraging results (Nikas and Iacovides, 2004). The low-*Re* terms, constants and damping functions have been determined with reference to fully-developed pipe flow and have not been changed in any of the subsequent applications.

Instead of the effective viscosity approximation, equation (4), the turbulent stresses are now obtained through the solution of separate transport equations, represented by equation (6) above. The transport of the turbulent stresses and also that of the dissipation rate ε, due to turbulent mixing, is modelled through the effective diffusivity concept. The term P_{ij} denotes the generation rate of the turbulent stresses and is obtained through the exact expression given equation (7). It is worth noting that the Coriolis force directly influences the generation rate of the Reynolds stresses. This effect obviously cannot be taken into account by effective viscosity models. In the most general case, the centrifugal force would also contribute to the generation rate of the Reynolds stresses. Because, however, the flow considered here is effectively a constant-density flow, the centrifugal terms are left out. The term ε_{ij} denotes the dissipation rate of the turbulent stresses which, as shown in equation (8), is assumed to be isotropic when the flow is fully turbulent and proportional to the ratio $\overline{u_i u_j}/k$ at the wall. The function f_ε is zero when the flow is fully turbulent and one at the wall.

The term ϕ_{ij}, given in equation (9), represents the redistribution of turbulent energy among the different components of the Reynolds stress tensor due to fluctuations in the pressure and strain fields. The first two terms denote a linear return to isotropy and isotropisation of production, respectively. They are also present in the widely used high-*Re* version of the DSM closure. Terms φ^w_{ij1}, and φ^w_{ij2}, given in equations (10)-(12), are the conventional wall reflection terms, proposed by Gibson and Launder (1978), to model the "wall-echo" part of the pressure strain correlation. Near solid surfaces, they remove kinetic energy from the fluctuating component normal to the wall and redistribute it in the other two directions. They have been devised for the * fully turbulent region of a flow over a plane wall and make use of the wall distance x_n and the unit vector normal to the wall n. Launder *et al.* (1975) propose defining x_n based on solid angles. This would, for example, increase turbulence damping in convex corner regions. Differential equation based distance functions that mimic the Launder *et al.* (1975) expression can be found in Tucker (2003). However, such issues are not explored here in the current Reynolds stress framework. Within the viscous sub-layer the wall reflection terms are damped through the function f_w. Their task within the viscous sub-layer is then performed by $(H_{ij} - H_{kk}\delta_{ij}/3)$, where H_{ij} is given by equation (13). The contribution of this term is more extensively discussed in Bo *et al.* (1995). It represents a relatively simple way of achieving approximately the correct distribution of the Reynolds stresses across the viscosity-affected sub-layer. The term J_{ij}, given in equation (14) increases the sensitivity of the model to the effects of low mean now Reynolds number. The turbulent heat fluxes are obtained through the generalised gradient diffusion hypothesis, given by equation (15).

Two-layer DSM closure. In the fully turbulent region, ε is obtained from the same equation used in the high-*Re* k-ε model:

$$\frac{\partial}{\partial x_j}(\rho U_j \varepsilon) = \frac{\partial}{\partial x_j}\left[\left(\mu + \frac{\mu_t}{\sigma_\varepsilon}\right)\frac{\partial \varepsilon}{\partial x_j}\right] + c_{\varepsilon_1}\frac{\varepsilon}{k}p_k - \rho c_{\varepsilon_2}\frac{\varepsilon^2}{k} \tag{16}$$

In the near-wall region, ε is obtained from the wall distance, as in the Wolfshtein (1969) model, $\varepsilon = k^{3/2}/l_\varepsilon$, but with:

$$l_e = 2.55Y[1 - \exp(-0.263y^*)] \tag{17}$$

The damping functions that appear in Equations (8)-(14) depend on the dimensionless wall distance y^* and have the following expressions:

$$f_e = \exp\left(\frac{-y^*}{3}\right) \tag{18}$$

$$f_w = [1 - \exp(-0.12y^*)][1 + \exp(-0.03y^*)] \tag{19}$$

$$f_J = 0.06\exp\left(\frac{-y^*}{3}\right) \tag{20}$$

$$f_H = (10.2 + 7.5y^*)\exp\left(\frac{-y^*}{20}\right) \tag{21}$$

Low-*Re* DSM closure. The dissipation rate equation is the same as that of the Low-*Re* k-ε model:

$$\frac{\partial}{\partial x_j}(\rho U_j \tilde{\varepsilon}) = \frac{\partial}{\partial x_j}\left[\left(\mu + \frac{\mu_t}{\sigma_\varepsilon}\right)\frac{\partial \tilde{\varepsilon}}{\partial x_j}\right] + c_{\varepsilon_1}\frac{\tilde{\varepsilon}}{k}p_k - \rho c_{\varepsilon_2} f_2 \frac{\tilde{\varepsilon}^2}{k} + 2\rho\nu v_t\left[\frac{\partial^2 U_i}{\partial x_j \partial w_q}\right]^2 \tag{22}$$

The damping function, f_2, which appears in previous equation (22), is: $f_2, = 1 - 0.3\exp(-R_t^2)$. As in the Launder and Sharma (1974) model, μ_t, is obtain from $\mu_1 = \rho c_\mu f_\mu k^2/\tilde{\varepsilon}$, with $f_\mu = \exp - 3.4/(1 + 0.02/R_t)^2$. The damping functions that appear in Equations (6)-(14) now depend on the turbulent Reynolds number, R_t have the following expressions:

$$f_e = \exp\left(\frac{-R_t}{8}\right) \tag{23}$$

$$f_w = \left[1 - \exp\left(\frac{-R_t}{20}\right)\right]\left[1 - \exp\left(\frac{-R_t}{100}\right)\right] \tag{24}$$

$$f_J = 0.06\exp\left(\frac{-R_t}{8}\right) \tag{25}$$

$$f_H = (10 + 2.6R_t)\exp\left(\frac{-R_t}{20}\right) \tag{26}$$

Also f_μ which still appears in the stress equation (6) and ε transport equations, is now obtained from:

$$f_\mu = \exp\left[\frac{-4}{(1+0.01R_t)^2}\right] \tag{27}$$

As mentioned earlier, the damping functions shown in Equations (18)-(21) and Equations (23)-(27) have been devised with reference to fully-developed pipe flows and not specifically for the ribbed passage flows presented in this study.

Length scale correction terms. In separated flows the Launder-Sharma version of the ε equation returns excessively high levels of near-wall turbulence. To address this problem Yap (1987) proposed the addition of a correction term to the ε equation, based on the wall distance, Y:

$$Yap = \max\left[0.83\frac{\tilde{\varepsilon}^2}{k}\left(\frac{k^{1.5}/\tilde{\varepsilon}}{2.55Y}-1\right)\left(\frac{k^{1.5}/\tilde{\varepsilon}}{2.55y}\right),0\right] \tag{28}$$

Iacovides and Raisee (1999) developed a differential form, by:

- introducing the magnitude of the resultant of the length scale ($\ell = k^{3/2}/\varepsilon$) gradient vector, $D\ell$; and
- also taking into account the effects of wall damping on the length scale as expressed by Wolfshtein (1969).

This leads to the following correction term NYap:

$$\mathrm{NYap} = \max\left[\frac{c_Y F(F+1)^2\rho\varepsilon^2}{k},0\right] \tag{29}$$

$$Dl = \left\{\left(\frac{\mathrm{d}l}{\mathrm{d}x_j}\right)\left(\frac{\mathrm{d}l}{\mathrm{d}x_j}\right)\right\}^{1/2} \tag{30}$$

and:

$$F = \frac{[Dl - (\mathrm{d}l_\varepsilon/\mathrm{d}Y)]}{c_l} \tag{31}$$

$$\left(\frac{\mathrm{d}l_\varepsilon}{\mathrm{d}Y}\right) = c_l[1-\exp(-B_\varepsilon R_t)] + B_\varepsilon c_l R_t \exp(-B_\varepsilon R_t) \tag{32}$$

With $c_l = 2.55$ and $B_\varepsilon = 0.1069$

Iacovides and Raisee (1999) initially suggested that $c\gamma$ should have the value of 0.83, as in the original Yap term, for both the low-*Re* k-ε and the low-*Re* DSM models. Here, following Craft (1998), who also adopted this term for his realisable DSM, for the low-*Re* DSM c_Y is set to 0.5. while for the low-*Re* k-ε it is left as 0.83.

The other modelling constants that appear in the preceding equations have the values given in Table I.

Table I. Turbulence modelling constants

c_μ	σ_k	σ_ε	$c_{\varepsilon 1}$	$c_{\varepsilon 2}$	c_1	C_2	c_1^w	c_2^w	c_T	σ_T
0.09	1	1.22	1.44	1.92	1.8	0.6	0.5	0.3	0.32	0.9

Numerical aspects

A three-dimensional non-orthogonal finite volume solver STREAM, has been employed, developed at UMIST, which employs the Cartesian velocity decomposition. A collocated grid is used. The SIMPLE algorithm is employed for the calculation of the pressure field, with the Rhie and Chow (1983) flux modification. In the case of the DSM models the apparent viscosity concept is used to prevent numerical oscillations that arise from the explicit presence of the Reynolds stress gradients in the momentum equations. What is done here is to effectively retain the effective viscosity formulation of the momentum transport equation and instead of using the real Reynolds stresses in the source terms the difference between the actual turbulent stresses and the stresses resulting from the EVM approximations, the apparent stresses, are employed. For the convective discretisation of all transport equations a bounded form of the quadratic upstream interpolation scheme (QUICK), was used, proposed by Iacovides (1999). For a given mesh, the DSM model required approximately twice as much storage and also twice the CPU time per iteration as the EVM model. Moreover, the DSM model required approximately twice, as many iterations as the EVM to reach a converged solution.

Cases examined

The case examined is that of a U-bend of square cross-section with a ratio between the inner radius of the bend and the duct diameter of 0.15. Flows at two Reynolds numbers ($U_{bl}/D/v$) have been computed, one at 100,000 and one at 36,000, both at a rotation number ($\Omega D/U_{bl}$) of 0.2. Heat transfer calculations have been obtained for a Prandtl number of 5.9, in order to match the experimental conditions. The flow domain started three-diameters before the bend and extended to eight diameters after the bend exit. The grid employed consisted of 58×58 grid nodes over the cross-section and 104 planes in the streamwise direction. In our recent study of flows through a stationary U-bend of the same geometry. Nikas and Iacovides (2004) computations with a mesh consisting of 45×86 grid nodes over the half cross-section and 104 streamwise planes produced the same flow and thermal predictions as a $31 \times 58 \times 104$ mesh. The latter mesh has same cross-sectional density as the one employed here. Ten – for the case of Re = 100,000 – and 15 – for Re = 36,000 – near-wall nodes fall in the one – equation sublayer. The y^* values adjacent to the walls are close to unity, ensuring that the near-wall nodes are positioned within the viscous sublayer and at the interface between the low- and high-*Re* regions are around 150, indicating that the low-*Re* region covers the entire viscosity-affected sub-layer.

Results and discussion

The measurements in Figure 2 show that, the orthogonal rotation has a strong influence on the flow development, within and downstream of the bend. The classical symmetric two-vortex structure within the bend is replaced by a single vortex, and after the bend, the flow along the inner wall separates only near the trailing side and accelerates near the leading side. It is well known (Bo *et al.*, 1995) that in the upstream section the Coriolis force increases the pressure along the trailing side relative to that of the leading side and also results in the transfer of the faster fluid along the trailing side, leaving the slower fluid along the leading side. Within the bend, as the main flow direction becomes parallel to the axis of rotation, the Coriolis force disappears, which

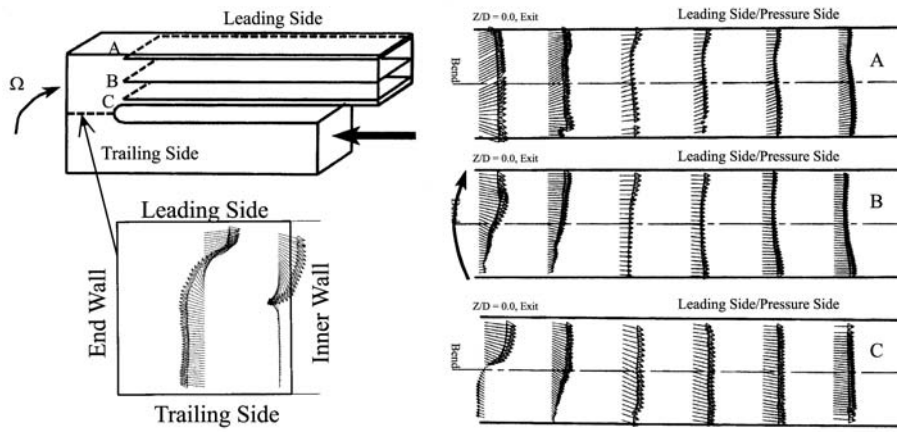

Source: Iacovides *et al.* (1999)

Figure 2.
Measured flow development

removes the difference in pressure between the leading and trailing sides. Consequently, as the fluid enters the bend it encounters a favourable pressure gradient along the trailing side and an adverse pressure gradient along the leading side. This in turn causes the single-vortex structure within the bend, seen in Figure 2, with strong flow separation along the leading side. The measurements at the bend exit and also flow visualization (Kelemenis, 1999) indicate that this single vortex is still present at the bend exit, causing the flow to separate only along the trailing side. As can be seen in Figure 3, the computations are able to reproduce the main features of the overall flow development. This is not unexpected because these are not turbulence driven phenomena. Moreover, the predicted secondary velocity vector plots of Figure 4,

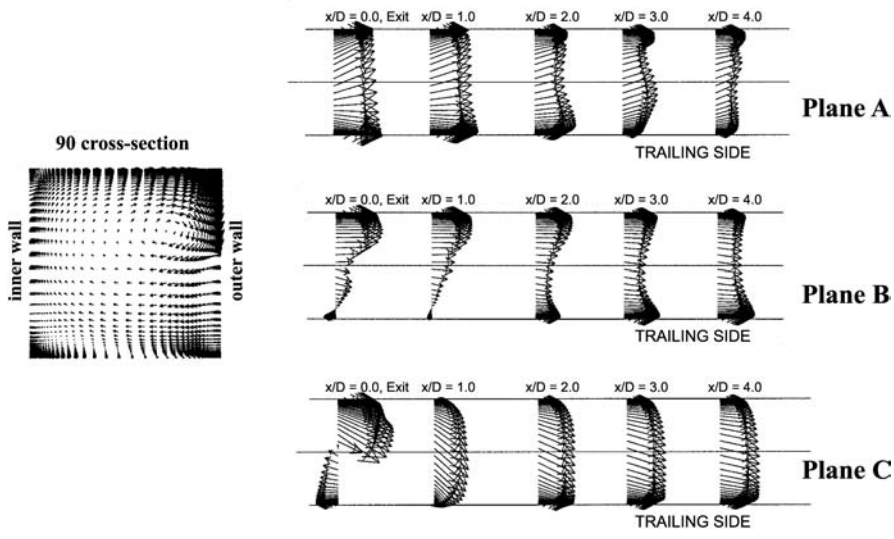

Figure 3.
Predicted flow development within and downstream of rotating bend, using the Low-*Re* DSM

also confirm the conclusion that the single vortex observed at the 90° plane is also present, with almost equal intensity, at the bend exit. Even two diameters after the exit this vortex is still present, though by this stage it has lost some of its strength.

Figure 5 shows more detailed comparisons of the axial velocity profiles along the mid-plane and also along planes near the inner and outer walls within and up to two diameters after the bend. Comparisons further downstream have not been included, because they show a close agreement between predictions and measurements. Along the outer wall, the different models used return very similar axial velocity predictions and at the bend exit and downstream (where measurements are available) there is very little difference between predictions and measurements. Along the mid-plane only small differences appear between the predictions of the low-*Re* and the two-layer models are still small. At the 90° location all models return a more gradual change in velocity across the duct than what is measured. Agreement between predictions and measurements improves at the end exit and the monitoring locations further downstream, but some small differences do persist along the trailing side. Along the inner wall, the comparisons now reveal that the predicted flow development within and just after the U-bend, becomes sensitive to the approach adopted for the modelling of near-wall turbulence. Use of two-layer models results in the under-prediction of the size of the separation bubble along the trailing side, within the bend, and also to a faster, than measured, recovery just downstream of it. The low-*Re* models produce mean flow predictions that are close to the measurements. Moreover, the differences between the low-*Re* effective-viscosity and second-moment closures are relatively minor. These findings are not surprising since along the inner wall the flow is subjected to an adverse pressure gradient which causes flow separation. It is thus reasonable to expect that the predictions of these more complex flow features will be sensitive to the modelling of near-wall turbulence and also that near-wall models that use the wall distance will be found to be inappropriate. On the whole both low-*Re* closures are in good, though not complete, agreement with the measured mean flow development.

The corresponding profile comparisons for the cross-duct velocity component, along the direction parallel to the axis of curvature, are shown in Figure 6. The positive values denote the direction from the leading to the trailing side. Along the outer wall again there are no differences in the predictions of the different models within and just after the bend. The measured cross-duct velocity, however, is somewhat stronger than that computed, especially along the trailing side. At the mid-plane, the data indicate that the magnitude of the cross-duct velocity becomes lower especially after the bend. There are still only minor differences among the computations of the various models, but there are now large discrepancies with the measured profiles especially within the bend. The cross-duct velocity is under-predicted and at the bend exit the predictions

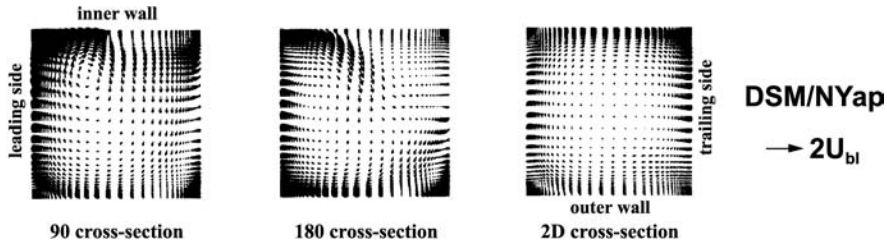

Figure 4.
Predicted secondary flow development

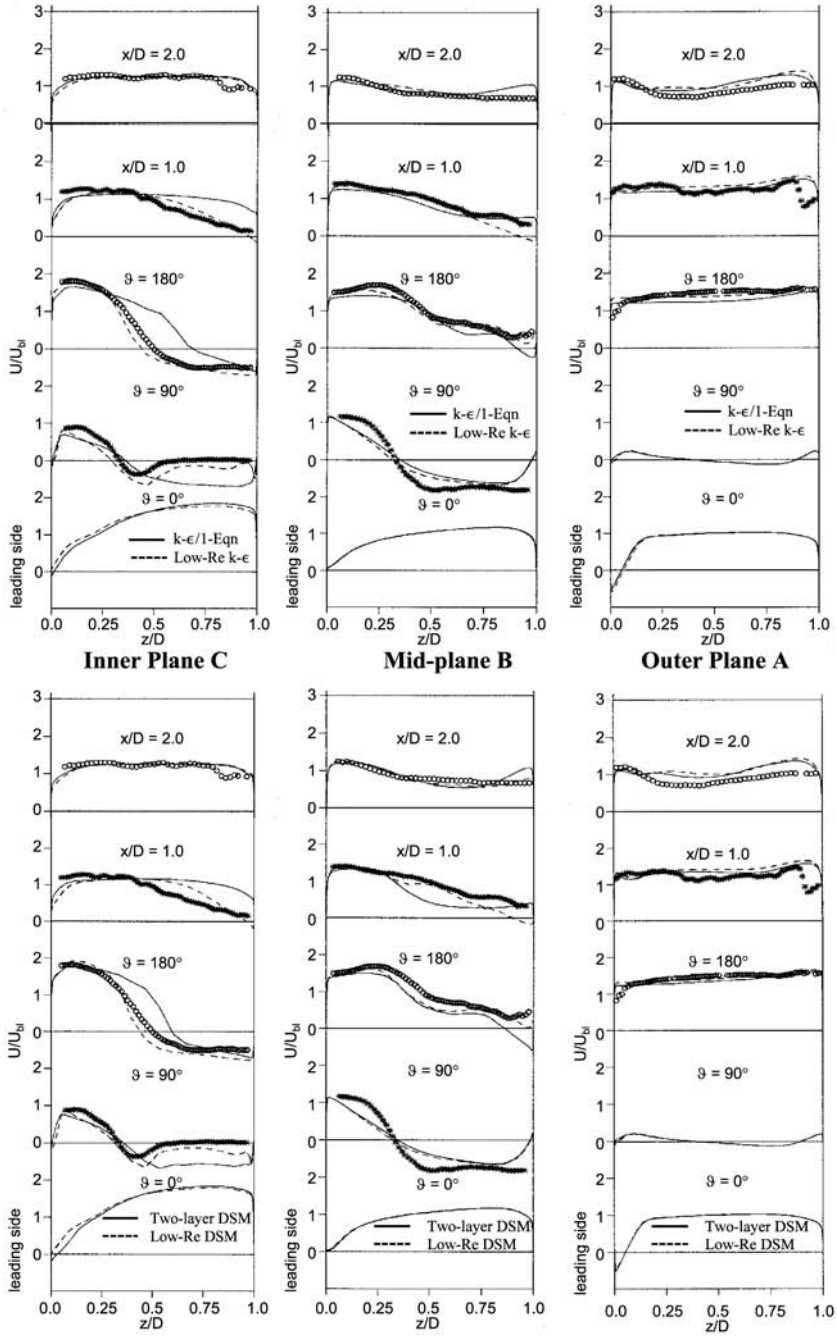

Note: ○○○○: Experiment
Source: Iacovides *et al.* (1996)

Figure 5.
Comparisons between predicted and measured profiles of mean streamwise velocity

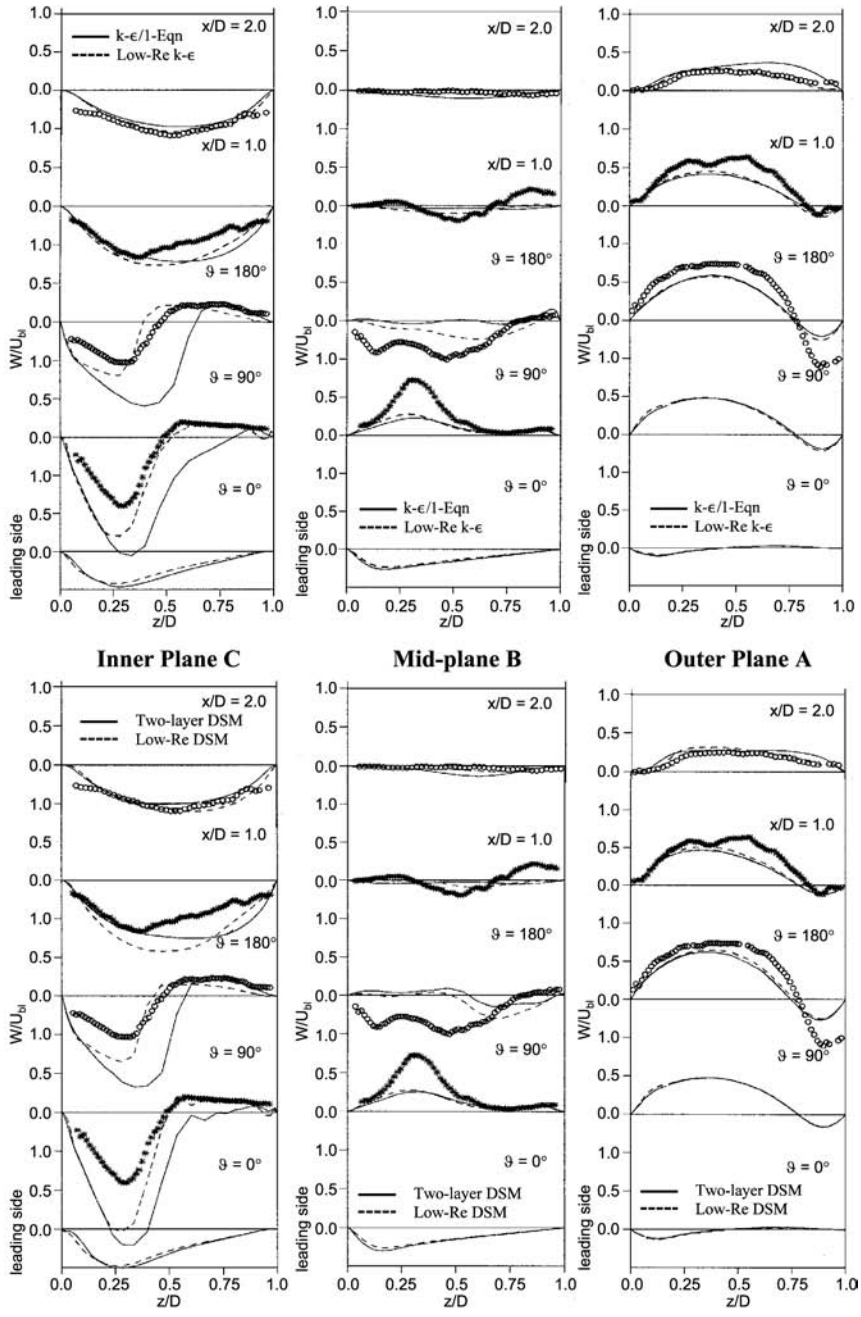

Note: ○○○○: Experiment
Source: Iacovides *et al.* (1996)

Figure 6.
Comparisons between predicted and measured profiles of mean cross-duct velocity

return also the wrong trends. Along the inner side, as also observed in the comparisons of the axial velocity, there are again large differences between the two-layer and the low-*Re* predictions, with the latter being closer to the data. The low-*Re* computations do not deviate from the data by as much as in the mid-plane comparisons, though within the bend, the cross-duct motion near the trailing side is over-predicted. It is thus found the cross-duct motion is better predicted along the inner and outer walls than at the mid-plane.

Figure 7 shows the corresponding comparisons for the cross-duct component of the turbulence intensity. The introduction of a second-moment closure has some effect on the predicted turbulence field. Within the bend, while all models return turbulence levels that are considerably higher than those of the upstream section, they still under-predict the measured high levels. This could be, though flow visualization studies reported, albeit briefly, in Iacovides *et al.* (1999) suggest that this is more relevant to the rotating case, because large-scale coherent flow components, that cannot be captured by the current RANS-based models, are present. Such features can be observed in the eddy resolving predictions of Chung and Tucker (2004) and are perhaps best dealt with using eddy resolving approaches suitable for high Reynolds number flows (Tucker and Davidson, 2004). However, such methods are computationally expensive. The distributions produced by the DSM models are closer to those measured than those of the EVM models. Along the near-inner-wall plane, as also noted in the mean velocity comparisons, there are noticeable differences between the predicted intensity levels of the low-*Re* models and those of the two-layer models. Downstream, as indicated by the comparisons at two diameters after the bend and also further downstream, not shown here due to space limitations, the measured turbulence levels become considerably lower and are well predicted by all the models tested. Moreover, the above comments are also largely applicable to the axial component of the turbulence intensity, for which, again due to space limitations, comparisons are not presented.

Finally, the assessment of the models tested is completed through the comparisons of the axial evolution of the side-averaged Nusselt number, shown in Figure 8. Here the comparisons produced by Nikas and Iacovides (2004) for the corresponding stationary case have also been included. This has been done in order to highlight the effects of rotation on wall heat transfer and also in order to provide a more complete assessment of the models' capabilities. The measurements show that in the stationary case the Nusselt number starts to increase inside the U-bend, reaching a maximum value of about twice that of the upstream section, about one diameter after the bend exit and then it starts to gradually fall. Along the trailing side rotation raises somewhat the Nusselt number levels, especially within and just after the bend, but does not change the overall variation. Along the leading side on the other hand, the effects of rotation are stronger. First, there is a much sharper rise in the Nusselt number at the bend entry where, as noted earlier, the interaction between the Coriolis and curvature forces leads to the formation of a stronger vortex. Then over the second half of the bend and also up to one and a half diameters after the exit there is a considerable reduction in wall heat transfer in comparison to both the stationary case and also the trailing side. This difference in the thermal behaviour of the two sides, is certainly consistent with the measured variation in the cross-duct turbulence intensity between the leading and trailing sides shown in Figure 7. For the stationary case the comparisons indicate that both the two-layer models produce a reasonable Nusselt number variation within and

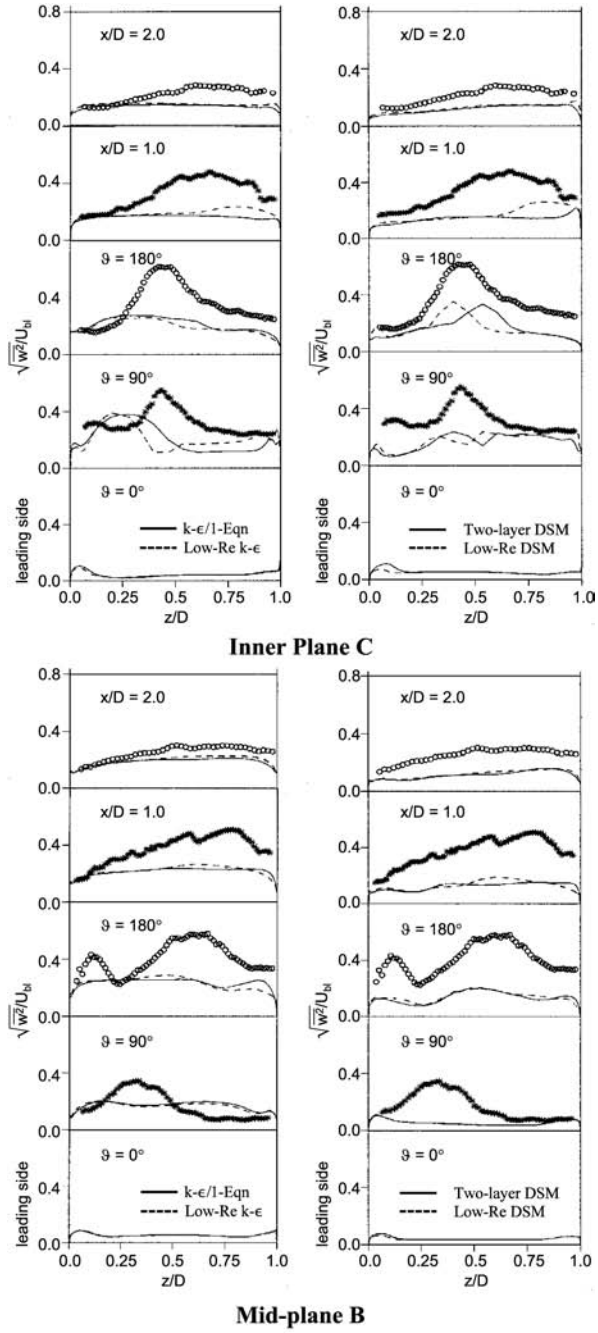

Note: ooooo: Experiment
Source: Iacovides *et al.* (1996)

Figure 7.
Comparisons between predicted and measured profiles of cross-duct turbulence intensity

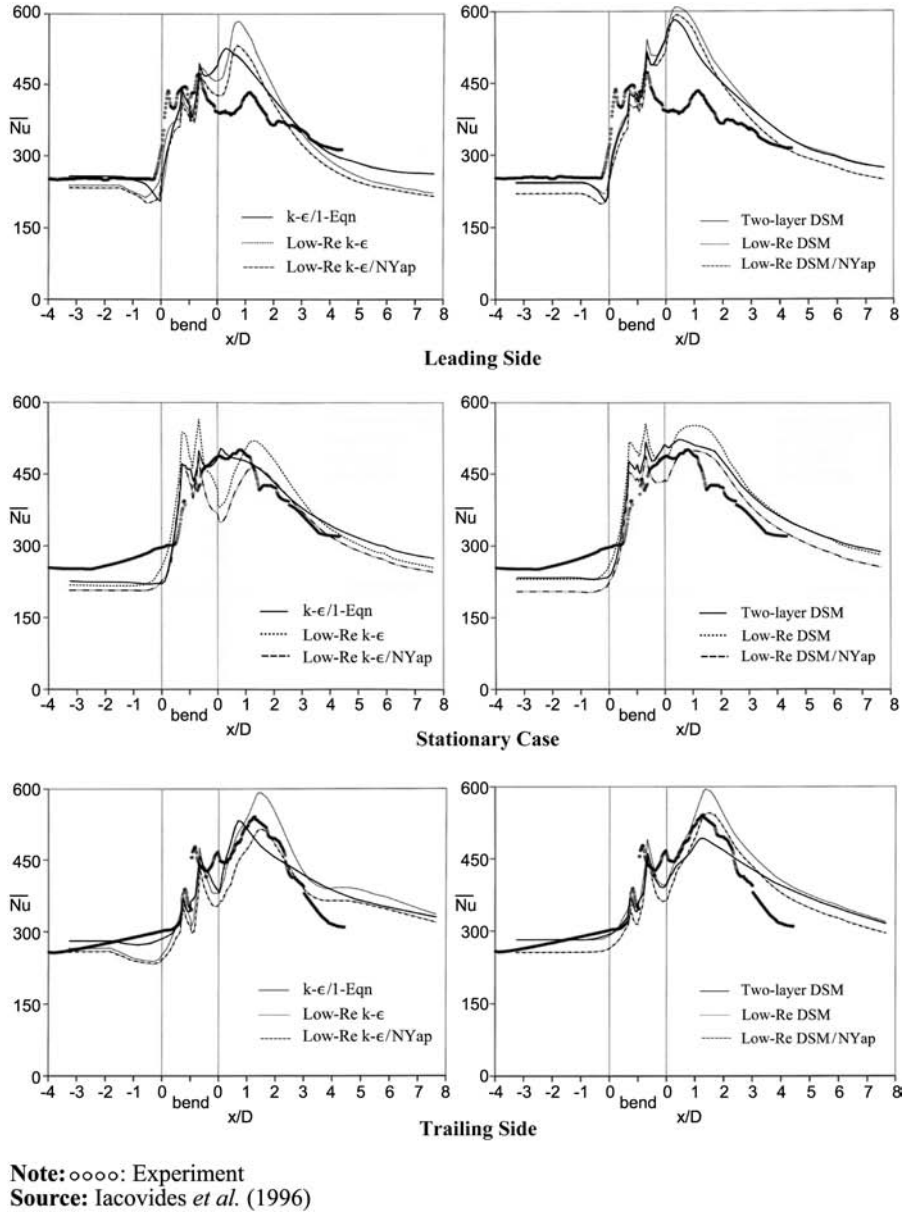

Note: ○○○○: Experiment
Source: Iacovides *et al.* (1996)

Figure 8.
Comparisons of the axial variation of the side-averaged Nusselt number along the flat wall for the stationary and rotating cases

after the bend, while as far as the low-Reynolds number models are concerned, only the low-*Re* DSM with the differential Yap term produces reasonable Nusselt number predictions. In the rotating case, along the trailing side, again none of the computations is in complete agreement with the measurements, but the predictions of

the low-*Re* DSM with the NYap, are closest to the data, returning the correct value and location of the maximum Nusselt number after the bend. Even this model, however, under-predicts heat transfer levels at the bend exit and also produces a reduction in wall heat transfer after the first two diameters which is too gradual in comparison to the data. The low-*Re* DSM with the Standard Yap term, in addition to the predictive deficiencies displayed by the version with the differential Yap term, Nyap, also over-predicts the peak heat transfer levels after the bend, while the zonal DSM under-predicts the peak heat transfer levels. The low-*Re* EVM models also under-predict heat transfer levels at the bend entry and within the bend, while the zonal EVM displays predictive deficiencies after the bend. Along the leading side, while all models successfully reproduce the sharp increase in Nusselt number at the bend entry, they fail to predict the drop in Nusselt number over the second half of the bend. This predictive deficiency is even more prominent in the DSM computations, though these models do come closer to predicting the correct recovery further downstream. Clearly the turbulence models find it very difficult to return the measured thermal behaviour, over the side along which the flow is most complex. Another point worth bearing in mind, is the effect of the molecular Prandtl number, which for water is greater than one, on the variation of the near-wall temperature and the consequences on the predictive effectiveness of the turbulence models. A Prandtl number higher than one, denotes that the molecular conduction of thermal energy is not as strong as the molecular diffusion of momentum. As a result, the conduction sub-layer, within which the turbulent heat flux becomes negligible in comparison to heat conduction, is considerably thinner than the hydrodynamic viscous sub-layer, where the turbulent transport of momentum is negligible in comparison to its molecular diffusion. The Nusselt number is thus more strongly influenced by the turbulence field in fluids with higher Prandtl number values. Consequently, the failure of turbulence models to return the correct near-wall turbulence field will have a greater detrimental effect on the thermal predictions. One positive outcome of these comparisons is that in the case of the low-*Re* DSM, the introduction of the differential form of the Yap term, which does not require the use of the wall distance, improves heat transfer predictions.

Concluding remarks

The heat and fluid flow computations carried out and the resulting comparisons lead to the following conclusions about the effectiveness of the EVM and DSM models tested in reproducing the flow and thermal development in rotating U-bends. The main flow features generated by the combined presence of rotation and curvature are well reproduced by all models. The detailed mean flow development within and just after the bend is better reproduced by low-*Re* rather than by two-layer models. Turbulence levels within the rotating U-bend are under-predicted, but DSM models produce a more realistic distribution. Along the leading side all models over-predict heat transfer levels just after the bend and along the trailing side the heat transfer predictions of the low-*Re* DSM with the differential Yap term, are reasonably close to the measurements. This model has also been found to lead to reasonable thermal predictions in a stationary U-bend of the same geometry. The introduction of the differential form of the length-scale correction term (NYap) tends to improve the heat transfer predictions of both low-*Re* models.

One class of models that has yet to be applied to the computation of these flows with such a strong engineering relevance are non-linear effective viscosity models, such as

those of Craft *et al.* (1996) and later adapted by Craft *et al.* (1999) and of Abid *et al.* (1996). These models combine the numerical robustness of linear EVM models with the ability to reproduce at least some of the non-isotropy of the turbulence field. As the recent work of Raisee *et al.* (2004a, b) has shown, the models developed by Craft and co-workers have already been tested in flows through curved ducts and in the prediction of heat transfer in separated flows. It would certainly be of value to establish how effective these models are in these more challenging test cases.

References

Abid, R., Morrison, H.J. and Gatski, T.B. (1996), "Prediction of aerodynamic flows with a new explicit algebraic stress model", *AIAA Journal*, Vol. 34 No. 12, pp. 2632-5.

Bo, T., Iacovides, H. and Launder, B.E. (1995), "Convective discretization schemes for the turbulence transport equations in flow predictions through sharp U-bends", *International Journal of Numerical Methods in Heat & Fluid Flow*, Vol. 5, pp. 33-48.

Chung, Y.M. and Tucker, P.G. (2004), "Numerical studies of heat transfer enhancements in laminar separated flows", *International Journal of Heat and Fluid Flow*, Vol. 25, pp. 22-31.

Craft, T.J. (1998), "Prediction of heat transfer in turbulent stagnation flow with a new second-moment closure", *Proc. 2nd Int. Conf. On Turbulent Heat Transfer, Vol. 2, 4.15-4.25, Manchester, UK*.

Craft, T.J., Iacovides, H. and Yoon, J.H. (1999), "Progress in the use of non-linear two-equation models in the computation of convective heat-transfer in impinging and separated flows", *Flow, Turbulence and Combustion*, Vol. 63, pp. 59-80.

Craft, T.J., Launder, B.E. and Suga, K. (1996), "Development and application of a cubic eddy-viscosity model of turbulence", *International Journal of Heat and Fluid Flow*, Vol. 17, pp. 108-15.

Ekkad, S.V. and Han, J.C. (1995), "Local heat transfer distributions near a sharp 180° turn of a two-pass smooth square channel using a transient liquid crystal image technique", *Journal of Flow Visualisation and Image Processing*, Vol. 2, pp. 285-97.

Gibson, M.M. and Launder, B.E. (1978), "Ground effects on pressure fluctuations in atmospheric boundary layers", *Journal of Fluid Mechanics*, Vol. 85, pp. 391-403.

Iacovides, H. (1999), "The computation of turbulent flow through stationary and rotating U-bends of with rib-roughened surfaces", *Int. J. on Numerical Methods in Fluids*, Vol. 29, pp. 865-76.

Iacovides, H. and Launder, B.E. (1992), "The computation of convective heat transfer in a 180° pipe bend", *Proc. ICHMT, Int. Symp. Heat Transfer in Turbomachinery, Athens*, pp. 541-52.

Iacovides, H. and Raisee, M. (1999), "Recent progress in the computation of flow and heat transfer in internat cooling passages of turbine blades", *International Journal of Heat and Fluid Flow*, Vol. 20, pp. 320-8.

Iacovides, H. and Raisee, M. (2001), "Computation of flow and heat transfer in two-dimensional rib-roughened passages, using low-Reynolds number turbulence models", *Int. J. Numerical Methods Heat and Fluid Flow*, Vol. 11, pp. 138-55.

Iacovides, H. and Toumpanakis, P. (1993), "Turbulence modelling of flow in axisymmetric rotor-stator systems", *Proc. IAHR, 5th Int. Symp. on Refined flow modelling and Turbulence Measurements*, pp. 835-42.

Iacovides, H., Launder, B.E. and Li, H-Y. (1995), "The computation of flow development through stationary and rotating U-bends of strong curvature", *International Journal of Heat and Fluid Flow*, Vol. 17, pp. 22-8.

Iacovides, H., Jackson, D.C., Launder, B.E. and Yuan, Y-M. (1996), "Flow measurements in stationary and orthogonally rotating smooth U-bend with rectangular outer wall", *Sponsors Report for ABB, EDF & EGT*, Department of Mechenical Engineering, UMIST, Manchester.

Iacovides, H., Jackson, D.C., Kelemenis, G., Launder, B.E. and Yuan, Y-M. (1999), "Experiments on local heat transfer in a rotating square-ended U-bend", *International Journal of Heat and Fluid Flow*, Vol. 20, pp. 302-10.

Kelemenis, G. (1999), "Flow and local thermal measurements in stationary and rotating cooling passages of complex geometries", PhD thesis, Faculty of technology, Mechanical Engineering Department UMIST, Manchester.

Launder, B.E. and Sharma, B.I. (1974), "Application of the energy-dissipation model of turbulence to the calculation of flow near a spinning disc", *Letters in Heat Mass Trans.*, Vol. 1, pp. 131-8.

Launder, B.E., Reece, G.J. and Rodi, W. (1975), "Progress in the development of a Reynolds-stress turbulence closure", *Journal of Fluid Mechanics*, Vol. 68 No. 3, pp. 537-66.

Nikas, K-S.P. and Iacovides, H. (2004), "The computation of flow and heat transfer through square-ended U-bends, using low-Reynolds-number models", *Int. J. of Numerical Methods for Heat & Fluid Flow*, Vol. 14 No. 3, pp. 305-24.

Raisee, M., Alemi, H. and Iacovides, H. (2004a), "Prediction of developing turbulent flow in a 90° curved duct, using linear and non-linear low-*Re* k-ε models", paper presented at ESDA2004-58466, 7th Biennial ASME Conference on Engineering Design and Analysis, Manchester.

Raisee, M., Noursadeghi, A. and Iacovides, H. (2004b), "Prediction of convective heat transfer through ribbed channels using a lowe-*Re* non-linear k-ε model", *Int. Journal for Numerical Methods in Heat and Fluid Flow*, Vol. 14 No. 3, pp. 285-304.

Rhie, C.M. and Chow, W.L. (1983), "Numerical study of the turbulent flow past an airfoil with trailing edge separation", *AIAA Journal*, Vol. 21 No. 11, pp. 1525-32.

Rigby, D.L., Ameri, A.A. and Steinhorsson, E. (1996), "Internal passage heat transfer prediction using multi block grids and k-ω turbulence model", ASME Paper, 96-GT-188.

Tucker, P.G. (2003), "Differential equation based wall distance computation for DES and RANS", *J. Computat. Phys.*, Vol. 190 No. 1, pp. 229-48.

Tucker, P.G. and Davidson (2004), "Zonal k-l based large eddy simulations", *Computers & Fluids*, Vol. 33, pp. 267-87.

Wolfshtein, M. (1969), "The velocity and temperature distribution in one-dimensional flow with turbulence augmentation and pressure gradient", *Int. J. Heat and Mass Transfer*, Vol. 12 No. 3, pp. 301-18.

Yap, C-R. (1987), "Turbulent heat and momentum transfer in recirculating and impinging flows", PhD thesis, Dept. of Mechanical Engineering, Faculty of Technology, University of Manchester, Manchester.

Corresponding author
Konstantinos-Stephen P. Nikas can be contacted at: mcjtpn4@fluid.mech.ntua.gr